Symmetry breaking mechanism for epithelial cell polarization

A. Veglio,[1,2] A. Gamba,[3,2,4] M. Nicodemi,[5,6] F. Bussolino,[1] and G. Serini[1]
[1]*Department of Oncological Sciences and Division of Vascular Biology, Institute for Cancer Research and Treatment, School of Medicine, University of Torino, Str. Prov. 142 Km. 3.95, 10060 Candiolo, Torino, Italy*
[2]*CNISM, Corso Duca degli Abruzzi 24, 10129 Torino, Italy*
[3]*Polytechnic of Torino, Corso Duca degli Abruzzi 24, 10129 Torino, Italy*
[4]*INFN, via Pietro Giuria 1, 10125 Torino, Italy*
[5]*Department of Physics and Complexity, Sciences, University of Warwick, Gibbet Hill Road, Coventry, CV4 7AL, UK*
[6]*INFN, via Cinita, 80126 Napoli, Italy*
(Received 8 August 2008; revised manuscript received 9 July 2009; published 29 September 2009)

In multicellular organisms, epithelial cells form layers separating compartments responsible for different physiological functions. At the early stage of epithelial layer formation, each cell of an aggregate defines an inner and an outer side by breaking the symmetry of its initial state, in a process known as epithelial polarization. By integrating recent biochemical and biophysical data with stochastic simulations of the relevant reaction-diffusion system, we provide evidence that epithelial cell polarization is a chemical phase-separation process induced by a local bistability in the signaling network at the level of the cell membrane. The early symmetry breaking event triggering phase separation is induced by adhesion-dependent mechanical forces localized in the point of convergence of cell surfaces when a threshold number of confluent cells is reached. The generality of the emerging phase-separation scenario is likely common to many processes of cell polarity formation.

DOI: 10.1103/PhysRevE.80.031919 PACS number(s): 87.17.Pq, 87.10.Tf, 87.15.K−, 87.17.Aa

I. INTRODUCTION

The development of epithelial tissues (e.g., kidney tubules, respiratory and gastrointestinal tracts, etc.) results from complex morphogenetic processes implying the arrangement of cells in layers organized along specific directional axes [1,2]. Epithelial cells are endowed with a self-polarization mechanism defining an "inner" and an "outer" side, which is mandatory to allow organs to exert their vital functions. In a well-established *in vitro* cell system, which recapitulates the *in vivo* morphogenesis, after a single epithelial cell is seeded in a three-dimensional gel [Fig. 1(a)], cell division begins and a multicellular aggregate arises [1]. The cells in the aggregate are bound each other [through cadherin molecules, Fig. 1(b)] and to an extracellular matrix [through integrin molecules, Fig. 1(c)]. When the cell number reaches five to six units, an inner cavity, named lumen, is spontaneously opened [3] [Figs. 1(a) and 1(b)]. Afterward, cells develop a top (called apical) and a bottom (basolateral) side [Fig. 1(d)] having different chemical features, while cell-cell and cell-matrix contacts only persist in the basolateral region. Finally, the border between apical and basolateral sides is sealed by ring-shaped tight junction proteins, which spontaneously find their functional position [Fig. 1(d)] and prevent intermixing of chemical components between the apical and the basolateral membranes, as well as the outpouring of liquids from the lumen. The full polarization process has a complex nature and involves different factors and stages. However, recent experiments have determined its master regulator (see [4,5] and references therein): intracellular asymmetry and lumen opening are controlled by PIP2 (phosphatydil-inositol 2 phosphate) and PIP3 (phosphatydil-inositol 3 phosphate) phospholipids (see Fig. 2) and their interaction with PTEN (phosphatase and tensin homolog) and PI3K (phosphatydil-inositol 3 kinase) enzymes which induce PIP2 and PIP3 segregation to opposite poles, while the PAR (partitioning-defective protein) complex further stabilizes axial polarity (see the review in [1] and references below). Even in such an *in vitro* system, however, the mechanism whereby the cell original spatial symmetry is spontaneously broken and polarization develops remains mysterious [1].

To describe cell differentiation, polarization, and signal localization mechanisms, stochastic reaction-diffusion [6] and coupled kinetic rate equations have been widely used for intracellular signaling, gene regulation, and autocatalytic reaction systems (see, e.g., [7–9] and references therein). In this context, here, we use reaction-diffusion equations to model the PIP2/3 master regulator in order to address some open questions [1], namely, the mechanisms for (i) the lumen site choice, (ii) its opening, (iii) the control of its final size, and (iv) the localization of tight junctions. After delineating the chemical reactions involved in the process, by simulation of its master equation we show that self-polarization can be understood in terms of statistical physics concepts as a symmetry breaking mechanism driven by the chemical regulatory network. We finally interpret the simulation results in terms of a simple mean-field model.

II. MODEL

Recent experiments have shown that PIP2 and PIP3 for a module that acts as a master regulator controlling all signaling pathways and cytoskeletal dynamics required for epithelial cell polarization [4,5]. PIP2/PIP3 levels are regulated by the counteracting enzymes PI3K and PTEN, which, respectively, catalyze the switch of PIP2 to PIP3, and vice versa [1,10] (Fig. 2). The phospholipids (PIP2/3) are stably local-

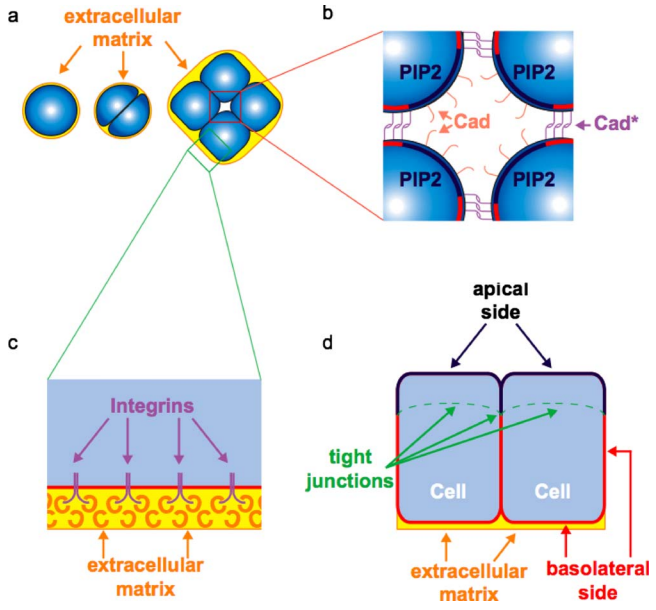

FIG. 1. (Color online) (a) and (b) After a few cell divisions, at the common point of contact among the cells of an aggregate, the intrinsic high membrane curvature locally induces the formation of a microlumen (inner circle) and the breaking of cell-cell adhesive receptor links (pink and purple bars). This breaking favors the appearance of a small region rich in PIP2 lipids (blue) which provides a nucleation center for the ensuing symmetry breaking process. (b) and (c) Everywhere but in correspondence of the PIP2-rich region, the cell is surrounded by adhesive contacts, either cell-cell (cadherins) or cell-matrix contacts (integrins). Cad (pink bars) and Cad* (purple bars), respectively, indicate inactive and active cadherins. (d) Scheme of the apical (blue) and basolateral (red) regions and the ring of tight junctions (green) spontaneously assembling at their interface. The extracellular matrix (yellow) is indicated as well.

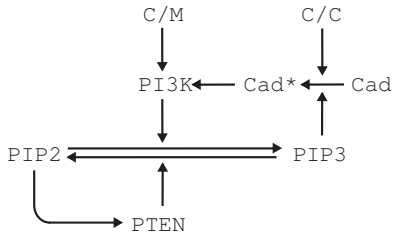

FIG. 2. Reactions scheme of the epithelial polarization network. The core players are the PI3K and the PTEN enzymes, which, respectively, catalyze the switch of the PIP2 lipid into PIP3, and vice versa. PTEN becomes effective upon association with PIP2, while PI3K becomes effective upon association with activated cell-cell adhesive receptors (cadherins, Cad*) or extracellular matrix adhesive receptors (C/M). To bind PI3K, cadherins (Cad) must be activated (Cad*) by linking other cadherins on neighboring cells (C/C) and by the action of PIP3. The symmetry of PTEN/PI3K in generating PIP2/3 can be broken by cadherins inactivation. The PIP2-PTEN feedback loop may then locally prevail, originating the chemical polarization of the cell.

ized in the inner face of the cell membrane where they diffuse. The enzymes (PI3K/PTEN) diffuse instead in the cell volume, where they are present in limiting amounts, and become active upon association with membrane spanning proteins or lipids. PTEN levels in the membrane are controlled by its binding to PIP2, thus realizing a positive feedback loop (see Fig. 2). PI3K levels in the membrane are controlled by its binding to cell-cell adhesive receptors (cadherins) and cell-matrix adhesive receptors (integrins, schematically indicated by C/M in Fig. 2) [11]. To bind PI3K, cadherins must be *activated* [Cad* in Figs. 1(b) and 2] by engagement with cadherins of a neighboring cell (named C/C in the diagram of Fig. 2); PI3K is active only when associated with either activated cadherins or integrins. Since PIP3 stabilizes the activated form Cad* [12], these interactions create a positive PIP3-PI3K feedback loop, mediated by the existence of cell-cell contacts (Fig. 2). Before polarization, cadherins and integrins are activated along the whole membrane and PIP3 uniformly prevails on PIP2 determining a stable PIP3-rich phase over the whole membrane. A local depletion of PIP3-PI3K can be created if a large enough membrane area with disrupted cell-cell links is formed, thereby breaking the PIP3-PI3K feedback loop (Fig. 2) and originating a germ of a PIP2-rich phase [Figs. 1(b) and 2]. Then, the PIP2-PTEN feedback loop may locally prevail, inducing a PIP2 and PIP3 surface compartmentalization that splits the cell membrane in two regions, or phases [13], characterized by different chemical concentrations of the signaling molecules.

Several mechanisms have been proposed [4] to explain the initiation of the polarization process, which is typically found in high curvature membrane regions, especially in correspondence of multiple cell-cell contacts (cellular vertex) [2] away from the extracellular matrix (Fig. 1). We observe here that cell-cell contacts can be broken [14] as soon as the adhesion energy W_a (i.e., the energy per unit area needed to break cadherin contacts) becomes comparable to the elastic energy stored in the cell membrane in high curvature regions, such as at the confluence of several cells [Figs. 1(a) and 1(b)]. Since the elastic energy per unit area W_e stored in the membrane is [15–17]

$$W_e = \kappa/2r^2, \tag{1}$$

where κ is the membrane bending rigidity and r is the local curvature radius [16], the condition $W_a \sim W_e$ allows us to estimate the critical curvature radius r_a where cell-cell contacts start being disrupted as [17]

$$r_a \simeq \sqrt{\kappa/2W_a}. \tag{2}$$

The critical value r_a can be easily estimated. In eukaryotic cells, the typical adhesion energy of cadherin contacts is $W_a \simeq 10^{-11}$ $\mu J/\mu m^2$ [17], while the typical bending rigidity is $\kappa \simeq 400 k_B T \simeq 16 \times 10^{-13}$ μJ [17], giving [18]

$$r_a \simeq 0.3 \ \mu m. \tag{3}$$

According to the above estimate, when the number of cells in the initial aggregate increases up to the five-to-six-cell stage, at the cell convergence points [see Fig. 1(b)], the membrane curvature increases as well and, especially in areas not in contact with the extracellular matrix, cadherin bridges are subjected to forces that can disrupt links. By such a mechanism, a local opening of cell-cell contacts breaks the PIP3-PI3K feedback loop and induces a local unbalance toward

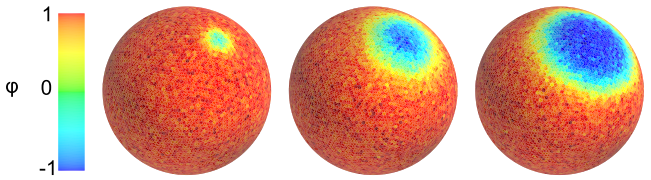

FIG. 3. (Color online) Growth of the PIP2-rich phase (blue upper patch). The color scale shows the gradation of PIP2 content: φ is the relative concentration difference between PIP3 and PIP2 at a given site. The system at initial time is in a uniform PIP3-rich phase, apart from an initial PIP2-rich seed germ of size r_0 larger than the threshold radius r_{thr} (small circle.) After 4 min a PIP2-rich patch becomes apparent and its radius saturates after approximately 10 min to the equilibrium value r_{eq}.

PIP2 formation (Fig. 2) and a germ of the PIP2-rich phase can be ushered in [Fig. 1(b)].

In Sec. III we show that only germs of the PIP2-rich phase larger than a threshold radius r_{thr} actually survive and grow. This fact suggests that, although the uniform PIP3-rich phase is not the more stable state for the signaling network, a polarized state characterized by the coexistence of the PIP3-rich and the PIP2-rich phases may be reached only by overcoming a barrier in a suitably defined effective energy (see Sec. IV for a detailed discussion of this point). Therefore, we are faced with the following physical picture: if elastic forces due to a high membrane curvature in the region of cell convergence (cellular vertex) trigger the disruption of cadherin links in a region of size larger than r_{thr}, the PIP2-rich patch grows favoring further breaking of cadherin links (Fig. 2) and the formation of a lumen. Thus, for the process of lumen formation to start, it is necessary that the local curvature radius in the cellular vertex satisfies

$$r_{\mathrm{a}} \gtrsim r_{\mathrm{thr}}. \tag{4}$$

The growth of the PIP2 patch and lumen slows down and eventually comes to a stop as soon as cytosolic PTEN is depleted. This way, at the end of the process the cell reaches a stable polarized state characterized by the coexistence of the PIP2-rich and the PIP3-rich phases [19,20], and a lumen coinciding with the PIP2-rich phase is formed.

III. SIMULATIONS

In this section we investigate on quantitative grounds the above-described scenario of polarization. Since the chemical reaction and diffusion processes are intrisically noisy, we simulate the corresponding dynamics by a stochastic algorithm, using realistic values for reaction and diffusion rates. We can check this way that noise alone is not sufficient here to overcome the energy barrier separating the uniform and polarized state in observational times, if an initial PIP2 seed of size larger than r_{thr} is not created by an external interaction.

We represent the plasma membrane by a lattice of $\mathcal{N}=10\,242$ (mostly hexagonal) sites of area $\sigma \sim S/\mathcal{N} \sim (0.1\ \mu\mathrm{m})^2$ on a sphere surface $S=4\pi R^2$ with radius $R=5\ \mu$m (Fig. 3). Each site is populated by a number

TABLE I. List of chemical reactions involved in epithelial polarization and their corresponding rates. X^* denotes the membrane-bound activated form of molecule X. Rate constants k are given in s^{-1}. Activation rates can be transformed to $(\mathrm{s\ M})^{-1}$ units by multiplying to Avogadro's number N_{A}. Michaelis-Menten constants K are pure numbers and can be transformed to M units by dividing to $N_{\mathrm{A}}/\mathcal{N}$. For the rate constants values see references in [21].

Reaction	W	Rate constants
$\mathrm{PIP2} \to \mathrm{PIP3}$	$k_1 N_{\mathrm{PIP2}} N_{\mathrm{PTEN}}/(K+N_{\mathrm{PIP2}})$	$k_1=1, K=50$
$\mathrm{PIP3} \to \mathrm{PIP2}$	$k_2 N_{\mathrm{PIP3}} N_{\mathrm{PI3K}}/(K+N_{\mathrm{PIP3}})$	$k_2=0.5, K=50$
$\mathrm{PTEN} \to \mathrm{PTEN}^*$	$k_3 N_{\mathrm{PTEN}} N_{\mathrm{PIP2}}$	$k_3=2\times10^{-5}$
$\mathrm{PTEN}^* \to \mathrm{PTEN}$	$k_4 N_{\mathrm{PTEN}^*}$	$k_4=0.5$
$\mathrm{PI3K} \to \mathrm{PI3K}^*$	$k_5 N_{\mathrm{PI3K}} N_{\mathrm{Cad}^*}$	$k_5=2\times10^{-5}$
$\mathrm{PI3K}^* \to \mathrm{PI3K}$	$k_6 N_{\mathrm{PI3K}^*}$	$k_6=0.1$
$\mathrm{Cad} \to \mathrm{Cad}^*$	$k_7 N_{\mathrm{Cad}} N_{\mathrm{PIP3}}$	$k_7=2\times10^{-5}$
$\mathrm{Cad}^* \to \mathrm{Cad}$	$k_8 N_{\mathrm{Cad}^*}$	$k_8=0.5$

of molecules of the chemical factors and their dynamics is described by standard master equations. For instance, the $\mathrm{PIP2} \to \mathrm{PIP3}$ process is described by

$$\begin{aligned}\partial_t P(N_{\mathrm{PIP}_2}, N_{\mathrm{PIP}_3}, \ldots) &= +W(\mathrm{PIP}_3 \to \mathrm{PIP}_2) P(N_{\mathrm{PIP}_2}-1, N_{\mathrm{PIP}_3}+1, \ldots) \\ &\quad - W(\mathrm{PIP}_2 \to \mathrm{PIP}_3) P(N_{\mathrm{PIP}_2}, N_{\mathrm{PIP}_3}, \ldots),\end{aligned} \tag{5}$$

where $P(N_{\mathrm{X}}, \ldots)$ is the probability to have at time t a number N_{X} of type X molecules at a given site (say, i.) The list of relevant reactions with their corresponding rates W is given in Table I [22]. PIP2/3 diffusion is described by random jumps of a molecule from site i to its neighboring site j with the rate $W(i \to j)=N_{\mathrm{X}} D/\sigma$, where $D=0.5\ \mu\mathrm{m}^2/\mathrm{s}$ is the phospholipid diffusivity [21]. Since the diffusivity of cytosolic enzymes (PI3K/PTEN) is much larger than that of membrane phospholipids [21], their distribution in the cytosol is treated as uniform.

For the simulations we use a variation of Gillespie algorithm [23] taking into account the spatial nonuniformity of the system. At time zero, a random number is generated to determine the next reaction or elementary diffusion process to occur, with a probability proportional to the corresponding W factor from Table I. Then, the time is advanced as a Poissonian process with a rate again determined by the W factors. These steps are repeated iteratively until the desired simulation time is reached.

We suppose that a circular PIP2-rich patch of radius r_0 is initially formed in the sea of the PIP3-rich phase [24] and investigate its dynamics to check whether a stable polarization state is attained (Fig. 3). Figure 4 shows the time evolution of circular patches of different initial radii r_0. Patches smaller than a threshold radius $r_{\mathrm{thr}} \sim 0.3\ \mu$m are dissolved by diffusion and thermal processes and do not impair the stability of the uniform PIP3-rich phase. Conversely, patches larger than r_{thr} grow in time triggering the separation of the cell surface in a PIP2-rich and a PIP3-rich region and eventually reach an equilibrium (Fig. 3). Notably, the threshold

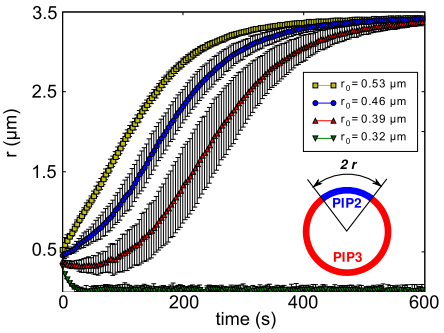

FIG. 4. (Color online) Growth of the PIP2-rich phase induced by a germ of initial radius r_0. Germs with r_0 smaller than a threshold radius $r_{\mathrm{thr}} \sim 0.3$ μm are melted by diffusion, while larger germs grow to the equilibrium value r_{eq}. Error bars show standard deviations computed over $n=50$ different random realizations of the process.

radius $r_{\mathrm{thr}} \sim$ 0.3 μm derived from the above calculation is consistent with the previously independently derived value for the adhesion radius r_{a}. The two phases are divided by an interface of characteristic width $\delta \sim \sqrt{D/k_{\mathrm{c}}} \sim 1$ μm [20], where k_{c} is on the order of the catalytic constants of the two catalytic reactions of Table I (first two rows).

The kinetic of this heterogeneous nucleation process can be understood in terms of nonequilibrium reaction-diffusion stochastic dynamics. In reaction-diffusion systems instabilities are often produced by Turing's mechanism [25]. Here, we find however that pattern formation starting from a locally stable homogeneous state is triggered by a local perturbation by a nucleation center of size r_0 larger than a critical size r_c [20,26–28].

Figure 5 shows that the equilibrium size r_{eq} of the PIP2-rich patch, and therefore of the lumen, is controlled by the number of PI3K and PTEN molecules. In the absence of any limiting mechanism, the growth of the PIP2-rich patch would in fact lead to a PIP2-rich phase completely invading the cell surface. However, due to the coupling to a finite PTEN and PI3K reservoir, the system self-tunes to a phase-coexistence state and the process stops when the PIP2-rich patch reaches

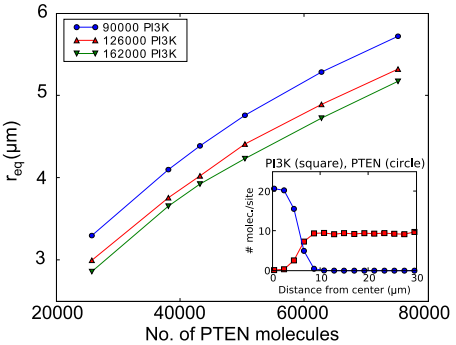

FIG. 5. (Color online) The equilibrium lumen size r_{eq} is an increasing function of the relative number of PI3K and PTEN molecules. Inset: radial distribution of PI3K (red squares, $N_{\mathrm{PI3K}}=1.26\times10^5$ molecules) and PTEN (blue circles, $N_{\mathrm{PTEN}}=0.43\times10^5$ molecules), from the patch center, at equilibrium.

the equilibrium size r_{eq} [19–21]. Interestingly, the fact that the size of the PIP2-rich patch, and consequently of the lumen, is controlled by the precise number of PTEN molecules is in qualitative agreement with the observation that deletion of a single PTEN allele can interfere with the polarization process [29].

The observation in the present scenario of a comparatively large threshold radius, on the order of one tenth of the cell size, suggests the existence of a correspondingly large barrier of effective energy dividing the uniform state from the phase-separated one. This prevents thermal and chemical noises from triggering spontaneous symmetry breaking and lumen formation. However, an external mechanical action creating a sizable PIP2-rich patch, due to the presence of localized regions of high membrane curvature, can overcome the barrier and start polarization [30]. Our picture also explains a tight junction localization. Experimental data show that the stable binding of tight junction proteins to the membrane requires both a protein complex named PAR3-PAR6, which is localized in the PIP2-rich phase by a chain of reactions, *and* cell-cell contacts, which are maintained only in the PIP3-rich phase [31]. The spontaneous aggregation of tight junctions is thus constrained by a biochemical logical AND to take place only on the ring-shaped boundary separating the PIP2-rich from the PIP3-rich phase.

IV. MEAN FIELD

In this section we show that the results of the simulations can be conveniently interpreted in terms of an effective mean-field model, following the approach detailed in Refs. [20,28]. The fast diffusion of PI3K and PTEN enzymes in the cytosol and the conservation law $[\mathrm{PIP2}]+[\mathrm{PIP3}]=c$ allow us to effectively describe the state of the cell membrane in terms of the configuration of the single-component concentration field as follows [20,28]:

$$\varphi = [\mathrm{PIP3}] - [\mathrm{PIP2}]. \tag{6}$$

The resulting effective equation for φ can be set in the simple Landau-Ginzburg form

$$\partial_t \varphi = D\nabla^2 \varphi + V'(\varphi) + \xi, \tag{7}$$

complemented by an integral constraint expressing the coupling of the concentration field φ to the reservoir of free cytosolic enzymes (see Refs. [20,28] and supplementary information in [21]) In Eq. (7), D is the diffusivity of lipids on the cell membrane, $V(\varphi)$ is an effective potential, and ξ is a stochastic term taking into account the effect of thermal and chemical noise.

The mean-field effective potential $V(\varphi)$ can be easily derived, via a quadratic approximation, from the stochastic model described in Sec. III under the assumption that the cytosolic PI3K, PTEN, and Cad fields are in approximate equilibrium with the membrane PIP2 and PIP3 fields, and therefore "slaved" to the φ field [20,28],

$$V'(\varphi) = -\alpha \frac{c^2 - \varphi^2}{2K + c + \varphi} + \alpha' \frac{c^2 - \varphi^2}{2K + c - \varphi}, \tag{8}$$

where

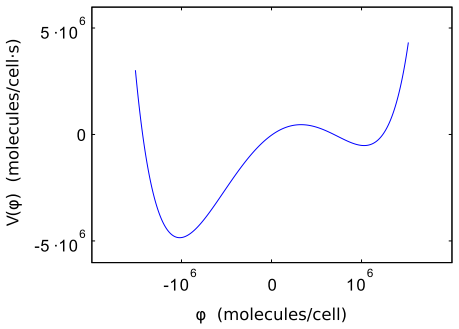

FIG. 6. (Color online) Graph of the effective potential $V(\varphi)$ defined by Eqs. (8)–(10), where the cytosolic values $[\mathrm{PTEN}]_{\mathrm{free}} \simeq 1.1 \times 10^4$, $[\mathrm{PI3K}]_{\mathrm{free}} \simeq 3.7 \times 10^4$, and $[\mathrm{Cad}]_{\mathrm{free}} \simeq 5.4 \times 10^3$ (molecules/cell) were computed from simulations of the stochastic model described in Sec. III at time $t=30$ s, after the fast equilibration of the corresponding cytosolic pools of enzymatic factors with the initial configuration of the φ field. The effective potential $V(\varphi)$ has two minima: the left-hand one corresponding to a stable PIP2-rich and the right-hand one corresponding to a metastable PIP3-rich phase. The two phases are separated by an effective energy barrier.

$$\alpha = \frac{k_2 k_3}{k_4}[\mathrm{PTEN}]_{\mathrm{free}}, \tag{9}$$

$$\alpha' = \frac{k_1 k_5}{k_6}[\mathrm{PI3K}]_{\mathrm{free}} \frac{k_7}{k_8}[\mathrm{Cad}]_{\mathrm{free}}. \tag{10}$$

The terms in the right-hand side of Eq. (8) describe, respectively, the conversion of PIP3 into PIP2 due to the action of PTEN and the conversion of PIP2 into PIP3 due to the action of PI3K activated by cadherins (Fig. 2). The quadratic terms $\propto c^2 - \varphi^2$ encode, respectively, the PIP2 $\rightarrow$ PTEN and the PIP3 $\rightarrow$ Cad $\rightarrow$ PI3K feedback loops (Fig. 2). In particular, $\alpha' = 0$ when cadherin links are broken.

In a wide region of parameter space around the realistic parameter values from Table I, the effective potential $V(\varphi)$ is bistable (Fig. 6; for a detailed description of the bistability region, see Ref. [32]). The two potential wells in Fig. 6 correspond to a stable PIP2-rich and a metastable PIP3-rich phase, separated by an energy barrier ΔV.

The mean-field model (7) and (8) and the bistability of the effective potential $V(\varphi)$ provide an interpretation to the simulation results, showing that the stable polarized state characterized by the coexistence of PIP2 and PIP3 in complementary regions is separated from the metastable PIP3-rich phase by an effective energy barrier ΔV. According to the theory of Landau-Ginzburg equation, PIP2-rich seeds larger than a critical value are bound to expand in the PIP3-rich sea with a velocity proportional to $1/\Delta V$ [26].

The cytosolic concentrations $[\mathrm{PI3K}]_{\mathrm{free}}$, $[\mathrm{PTEN}]_{\mathrm{free}}$, and $[\mathrm{Cad}]_{\mathrm{free}}$ appearing in Eq. (8) may be expressed as integrals of the concentration field φ [28,32]. The resulting global coupling has the effect of driving dynamically the cell membrane toward an equilibrium polarized state where the PIP2-rich and PIP3-rich phases coexist: the growth of the PIP2-rich phase "eats up" free PTEN molecules from the cytosol, decreasing ΔV until phase coexistence is reached [28,32]. This process may be understood via a simple physical analogy with the nonequilibrium process taking place during the liquid-vapor transition in a sealed vessel: there, the rise of the vapor pressure (which in our analogy corresponds to the number of cytosolic enzymes) provides a negative feedback, slowing down the growth of the vapor phase and eventually leading the system to a state of phase coexistence. The main difference between the two systems is that in the liquid-vapor transition a local conservation law holds for the particle field, while in the growth of signaling domains on the cell membrane the φ field satisfies only an approximate *global* constraint [28] encoded in the integral expressions for the coefficients α, α' appearing in Eqs. (8)–(10).

It is worth observing here that while spontaneous polarization in eukaryotic directional sensing [21] can be described in terms of an homogeneous nucleation process, whereby seeds of a PIP3-rich phase are created by thermal and chemical noises in the sea of the PIP2-rich phase and grow by a coarsening process [20,28], the present picture of epithelial polarization reminds instead a *heterogeneous* nucleation, i.e., a situation where the effective potential barrier ΔV is so high that spontaneous nucleation does not occur in typical observational times and needs to be triggered by the introduction of a large enough nucleation germ.

V. DISCUSSION

We have shown that a simple symmetry breaking mechanism, informed with the recently discovered biochemical and biophysical details of the system, accounts for a wealth of morphogenetic processes in epithelial polarization. The model makes specific predictions on the dependence of the threshold radius, the lumen size, the tight junction positioning, and the width on the biochemical system parameters. Our results shed light on the role of PTEN as a tumor suppressor protein, whose expression levels are known to be critical to prevent the onset of cancer. In particular, our models predict that, by decreasing the number of PTEN molecules, the lumen size should decrease, and for very low PTEN levels no lumen at all should form. The experimental validation of the model could be performed by genetic manipulation of the amounts or activity of cadherins, PI3K, and PTEN.

We have also shown that curvature-induced forces are a very plausible candidate for triggering the symmetry breaking process at the right time. This could be verified experimentally by trying to induce localized formation of a growing PIP2 patch and lumen by mechanically breaking adhesion bonds in localized regions of the membrane of epithelial cells surrounded by extracellular matrix. Under these conditions, our model predicts that only breaking adhesion bonds in regions larger than r_{thr} should induce the formation of a growing patch of the PIP2-rich phase, while smaller PIP2-rich patches, induced by breaking adhesive bonds on smaller regions, should shrink spontaneously.

Interestingly, the bistable PI3K-PTEN module described here plays also a key role in chemotaxis, where PI3K is initially activated by chemotactic receptors (see the review in

[33] and references therein) rather than by adhesive receptors. While experimental evidences and our results suggest that epithelial polarization is induced by a nucleation center of the PIP2-rich phase generated by mechanical forces, the polarization of migrating cells is likely to be triggered by spontaneous fluctuations in PIP3/PI3K levels [20].

The PIP3 localization also regulates the chemotactic polarization [20,21] and the cell spindle orientation [34]. The similarity underlying the mechanisms in these very different aspects of cell life hints to the possibility that phase-separation phenomena might have a general role in the cell [20,21] and in its nucleus [35,36]. The principles emerging here could explain in a universal way the deep analogies observed in a variety of cellular processes involving spatial polarity formation [1,37–40].

ACKNOWLEDGMENTS

We thank G. Boffetta for discussions, hospitality at ISAC-CNR and access to computational facilities, and S. Vegetti for suggestions. This work was partially supported by Telethon–Italy Contract No. GGP04127, AIRC, MIUR (PRIN Contract No. 2007BMZ8WA), Regione Piemonte, PRESTO, Fondazione CRT, and Ministero della Salute.

[1] F. Comer and C. Parent, Cell **128**, 239 (2007).
[2] F. Martin-Belmonte, A. Gassama, A. Datta, W. Yu, U. Rescher, V. Gerke, and K. Mostov, Cell **128**, 383 (2007).
[3] A. Z. Wang, G. K. Ojakian, and W. J. Nelson, J. Cell Sci. **95**, 137 (1990).
[4] D. M. Bryant and K. E. Mostov, Nat. Rev. Mol. Cell Biol. **9**, 887 (2008).
[5] I. Mellman and W. J. Nelson, Nat. Rev. Mol. Cell Biol. **9**, 833 (2008).
[6] N. van Kampen, *Stochastic Processes in Physics and Chemistry*, 3rd ed. (North-Holland, Amsterdam, 2007).
[7] S. Ramanathan, P. B. Detwiler, A. M. Sengupta, and B. I. Shraiman, Biophys. J. **88**, 3063 (2005).
[8] M. Thattai and A. van Oudenaarden, Biophys. J. **82**, 2943 (2002).
[9] J. Paulsson, O. G. Berg, and M. Ehrenberg, Proc. Natl. Acad. Sci. U.S.A. **97**, 7148 (2000).
[10] V. Kölsch, P. G. Charest, and R. A. Firtel, J. Cell Sci. **121**, 551 (2008).
[11] S. J. Watton and J. Downward, Curr. Biol. **9**, 433 (1999).
[12] A. S. Yap and E. M. Kovacs, J. Cell Biol. **160**, 11 (2003).
[13] L. Landau and E. Lifshitz, *Course of Theoretical Physics* (Butterworth-Heinemann, Burlington, MA 1980), Vol. 5.
[14] R. Kroschewski, News Physiol. Sci. **19**, 61 (2004).
[15] L. Landau and E. Lifshitz, *Course of Theoretical Physics* (Butterworth-Heinemann, Burlington, MA, 1986), Vol. 7.
[16] J. Fournier, Soft Matter **3**, 883 (2007).
[17] R. Simson, E. Wallraff, J. Faix, J. Niewöhner, G. Gerisch, and E. Sackmann, Biophys. J. **74**, 514 (1998).
[18] It is worth observing here that since the values κ and W_a used for the estimate have been measured on live cells [17], they take effectively into account the mechanical contributions from both the lipid bilayer and the cortical cytoskeleton.
[19] T. Ferraro, A. de Candia, A. Gamba, and A. Coniglio, EPL **83**, 50009 (2008).
[20] A. Gamba, I. Kolokolov, V. Lebedev, and G. Ortenzi, Phys. Rev. Lett. **99**, 158101 (2007).
[21] A. Gamba, A. de Candia, S. D. Talia, A. Coniglio, F. Bussolino, and G. Serini, Proc. Natl. Acad. Sci. U.S.A. **102**, 16927 (2005).
[22] The values for processes involving cadherins are educated guesses since no precise data are available. One order of magnitude changes in these values do not result however in appreciable modifications of the system dynamics.
[23] D. T. Gillespie, J. Phys. Chem. **81**, 2340 (1977).
[24] Where not otherwise stated, the following experimentally realistic values for the initial concentration are used: [PIP2]+[PIP3]=10^6 (according to [37]), [PI3K]=[Cad]=10^5 (according to [38,39], respectively), and [PTEN]=0.2×10^5 (molecules/cell). For the PTEN concentration, we assumed the same order of magnitude as in [21] and studied in Fig. 5 the system behavior on varying the PTEN molecules number. The initial PIP3-rich phase is 98% PIP3 and 2% PIP2.
[25] A. M. Turing, Philos. Trans. R. Soc. London, Ser. B **237**, 37 (1952).
[26] A. Bray, Adv. Phys. **43**, 357 (1994).
[27] E. Schöll, *Stochastic Processes in Physics, Chemistry, and Biology* (Springer, New York, 2000), pp. 437–451.
[28] A. Gamba, I. Kolokolov, V. Lebedev, and G. Ortenzi, J. Stat. Mech.: Theory Exp. (2009) P02019.
[29] A. Gassama-Diagne, W. Yu, M. ter Beest, F. Martin-Belmonte, A. Kierbel, J. Engel, and K. Mostov, Nat. Cell Biol. **8**, 963 (2006).
[30] Interestingly, the role of mechanical forces has been suggested also in other settings of tissue morphogenesis [40].
[31] B. Margolis and J.-P. Borg, J. Cell Sci. **118**, 5157 (2005).
[32] A. Gamba, G. Naldi, M. Semplice, G. Serini, and A. Veglio (unpublished).
[33] P. A. Iglesias and P. N. Devreotes, Curr. Opin. Cell Biol. **20**, 35 (2008).
[34] F. Toyoshima, S. Matsumura, H. Morimoto, M. Mitsushima, and E. Nishida, Dev. Cell **13**, 796 (2007).
[35] M. Nicodemi and A. Prisco, Phys. Rev. Lett. **98**, 108104 (2007).
[36] M. Nicodemi, B. Panning, and A. Prisco, Genetics **179**, 717 (2008).
[37] B. Vanhaesebroeck, S. J. Leevers, K. Ahmadi, J. Timms, R. Katso, P. C. Driscoll, R. Woscholski, P. J. Parker, and M. D. Waterfield, Annu. Rev. Biochem. **70**, 535 (2001).
[38] C. L. Carpenter, B. C. Duckworth, K. R. Auger, B. Cohen, B. S. Schaffhausen, and L. C. Cantley, J. Biol. Chem. **265**, 19704 (1990).
[39] D. Duguay, R. A. Foty, and M. S. Steinberg, Dev. Biol. **253**, 309 (2003).
[40] B. I. Shraiman, Proc. Natl. Acad. Sci. U.S.A. **102**, 3318 (2005).